THE DYNAMIC STABILITY AND NON-LINEAR RESONANCE OF A FLEXIBLE CONNECTING ROD: SINGLE-MODE MODEL

S.-R. HSIEH AND S. W. SHAW

Department of Mechanical Engineering and Applied Mechanics, University of Michigan, Ann Arbor, Michigan 48109-2125, U.S.A.

An analytical and computer simulation investigation of the dynamic behavior associated with the flexible connecting rod of an otherwise rigid, in-line, planar slider–crank mechanism is presented. The main goal of this work is to determine the manner in which this response depends on the system parameters, with a particular emphasis on non-linear analyses of the dynamic response near resonance conditions. A single-mode model is distilled from the governing partial equations and is used to describe the transverse deflection of the connecting rod. It is found that the slider mass is the primary source of the non-linearity, and that the connecting rod behaves as a system with a softening type of non-linearity, which is subjected to both external and parametric excitations. The effects of selected non-dimensional system parameters, such as the length ratio, damping ratios, frequency ratios and inertia ratios, are investigated in detail. A systematic numerical study is also carried out and compared with the analytical results.

1. INTRODUCTION

High operating speeds, superior reliability and accurate performance are major characteristics of modern industrial machinery and commercial equipment. A traditional rigid body analysis, which presumes low operating speeds, becomes insufficient to describe the performance of such high speed machinery. A thorough understanding of the dynamic behavior of machine elements undergoing high speed operations is necessary in these situations. It is the purpose of this investigation to present an analytical approach for describing the dynamic response of an elastic mechanism element and provide a theoretical explanation for some of the dynamic phenomena observed in both numerical and experimental studies [1–4]. One of the simplest and most common mechanisms, the slider–crank mechanism, is selected as the prototype system to demonstrate this analytical work.

In this investigation, the vibration associated with a flexible connecting rod of an otherwise rigid, in-line, planar slider–crank mechanism is considered. This problem is equivalent to determining the flexural response of a simply supported beam which is subjected to (1) support motion which arises from the motion of the crank shaft and the kinematic constraints of the mechanism, and (2) an axial load arising from forces applied to the slider mass and the inertial force of the slider mass.

Similar systems have been investigated by several authors. A brief survey of some relevant papers is given below. More complete information is found in the series of review articles provided in references [5–8].

Neubauer, Cohen and Hall [9] examined the transverse deflection of an elastic connecting rod of a slider–crank mechanism by neglecting the longitudinal deformation,

25

the Coriolis, relative tangential and relative normal components of acceleration. By using the method of averaging and assuming a small length ratio, Jasinski *et al.* [10, 11] investigated the dynamic stability of a flexible connecting rod in a slider–crack mechanism. Viscomi and Ayre [4] examined the non-linear bending response of the connecting rod, using simulations of single- and multi-mode models. By applying a regular perturbation method to Euler–Bernouli and Timoshenko beam models, Badlani and Kleinhenz [12] considered the dynamic stability of the undamped elastic connecting rod of an in-line slider–crank, and compared the results from each approach. Tadjbakhsh [13] introduced a general method for obtaining a single partial differential equation describing the transverse vibration of an undamped elastic link of a mechanism which contains evolutes only, using a two-parameter perturbation approach. Zhu and Chen [14] studied the stability of the response of the connecting rod by using a regular perturbation technique. Badlani and Midha [15] studied the effect of internal material damping on the dynamic response behavior of a slider–crank mechanism by using a regular perturbation method. Beale and Lee [16] studied the motion of the flexible connecting rod of a slider–crank mechanism with a direct variational approach. Farhang and Midha [17] have carried out a detailed study of the parameter regions in which parametric instabilities can occur in this system, and have included several modes in their study. Additional results on parametric instabilities in mechanisms can be found in the work of Midha and co-workers [18–20].

In addition to the analytical and computational works described above, some experimental work has been carried out. Golebiewski and Sadler [2] analytically and experimentally determined the bending stress at the mid-point of an elastic connecting rod. Beale *et al.* have recently carried out an experimental study of a system very similar to the one considered herein, and found responses consistent with their analysis [21] and the present work. Sutherland [3] studied a fully elastic, planar four-bar mechanism analytically and experimentally.

Most previous stability investigations have considered a non-homogeneous Mathieu equation to describe the stability of transverse vibrations, and only linear stability analyses were provided. The existence of superharmonic, subharmonic and combination resonances has been observed both in simulations and experiments [1–4]. A numerical study of the overall non-linear response, especially dealing with the superharmonic, subharmonic responses and their associated stability, is given by Beale *et al.* [16, 21]. The purpose of this study is to provide a complementary analytical study. This work focuses on the non-linear aspects of the dynamic response, including primary, principal parametric, superharmonic and subharmonic resonances and their stability.

In the course of this study, extensive use was made of the computer-assisted symbolic manipulation program *Mathematica*™. This was essential in the length calculations involved in the perturbation procedures. In a companion paper [22], the authors provide a detailed investigation of a continuous parameter model of the same system, which includes the effects of shear deformations and rotary inertia.

This paper is organized as follows. Section 2 contains the basic assumptions and the derivation of the differential equation of motion. Section 3 provides the analysis of this equation using the method of multiple scales. Section 4 contains detailed numerical simulations for this model and a discussion of the effects of several dimensionless parameters on the response. The paper is closed with some conclusions in section 5.

2. EQUATION OF MOTION

In this section, an equation describing the first mode flexural vibration associated with the flexible connecting rod of an otherwise rigid, in-line, planar slider–crank mechanism

is derived by using Euler–Bernoulli beam theory and a shadow-beam formulation [23–25]. The connecting rod AB depicted in Figure 1 is assumed to be uniform and made of a viscoelastic material (Kelvin–Voigt material [15]), and is simply supported at both pivots (points A and B). The crank element OA is assumed to be perfectly rigid, and operating with constant angular speed ω. The slider mass has no clearance and no offset. There is no external (piston) force applied to the slider mass. The OXY co-ordinate system represents a fixed inertial reference frame, with its origin attached to the rotation center of the crank shaft. The oxy co-ordinate system represents a moving reference frame with its origin attached at joint A and the ox axis passing through the ideal pin joints at the ends of the undeformed connecting rod; it makes an angle $-\phi$ with respect to the OX axis. Let $u(x, t)$ and $v(x, t)$ represent the axial and transverse displacements of the connecting rod in the x and y directions, respectively. Based on previous assumptions, the equations of motion in the oxy co-ordinate system are

$$\partial P(x, t)/\partial x = EA\,(u_x + \tfrac{1}{2}v_x^2)_x + A\mu_c(u_x + \tfrac{1}{2}v_x^2)_{xt} = \rho A a_x, \tag{1}$$

$$EIv_{xxxx} + I\mu_c v_{xxxxt} - EA\,[(u_x + \tfrac{1}{2}v_x^2)_x v_x]_x - \mu_c A\,[(u_x + \tfrac{1}{2}v_x^2)_t v_x]_x = \rho A a_y, \tag{2}$$

where $P(x, t)$ is the axial force acting on the connecting rod along the x-direction, I is the area moment of inertia of the connecting rod, E is the Young's modulus, ρ is the mass density (mass per unit volume), A is the cross-sectional area, μ_c is the internal material damping coefficient, and $a_x(x, t)$ and $a_y(x, t)$ are the acceleration components of a material element. These are given by

$$a_x = -r\omega^2 \cos(\omega t - \phi) + \frac{\partial^2 u}{\partial t^2} - 2\frac{\partial \phi}{\partial t}\frac{\partial v}{\partial t} - \frac{\partial^2 \phi}{\partial t^2}v - \left(\frac{\partial \phi}{\partial t}\right)^2(x + u), \tag{3}$$

$$a_y = -r\omega^2 \sin(\omega t - \phi) + \frac{\partial^2 \phi}{\partial t^2}(x + u) + 2\frac{\partial \phi}{\partial t}\frac{\partial u}{\partial t} + \frac{\partial^2 v}{\partial t^2} - \left(\frac{\partial \phi}{\partial t}\right)^2 v. \tag{4}$$

Previous investigations [15] have shown that the axial displacement is small compared to the transverse displacement. Therefore, we neglect the contribution of the axial displacement on the inertia forces $\rho A a_x$ and $\rho A a_y$. Equation (1), then, becomes

$$\frac{\partial P}{\partial x} = EA\,(u_x + \tfrac{1}{2}v_x^2)_x + A\mu_c(u_x + \tfrac{1}{2}v_x^2)_{xt}$$

$$= \rho A\left[-r\omega^2 \cos(\omega t - \phi) - 2\left(\frac{\partial \phi}{\partial t}\right)\left(\frac{\partial v}{\partial t}\right) - \frac{\partial^2 \phi}{\partial t^2}v - \left(\frac{\partial \phi}{\partial t}\right)^2 x\right]. \tag{5}$$
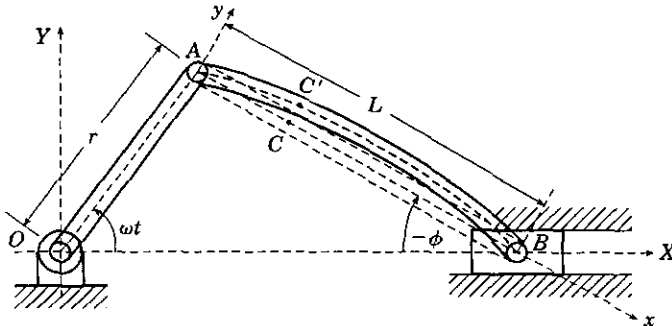

Figure 1. Slider–crank mechanism with flexible connecting rod (deformed state). The effects of foreshortening are not depicted.

Integrating equation (5) from 0 to x, the axial force in the connecting rod is obtained as

$$P(x, t) = P(0, t) + \rho A \int_0^x a_x \, dx, \tag{6}$$

where $P(0, t)$ represents the force applied to the end of the connecting rod to which the end mass m_4 is attached. Using Figure 1 and summing forces along the x-direction [4], the time-varying axial force $P(x, t)$ is determined to be

$$P(x, t) = \rho A \int_L^x a_x \, dz + m_4 \ddot{\delta} + \mu_s \dot{\delta} + \rho A (\tan \phi / L) \int_0^L (a_y x - a_x v) \, dx - (m_4 \ddot{Z}(t)$$
$$+ \mu_s \dot{Z}(t)) / \cos \phi, \tag{7}$$

where an overdot represents a time derivative, L denotes the length of the connecting rod, $\ddot{Z}(t)$ represents the contribution of the piston acceleration from the rigid body motion of the mechanism, $\mu_s \dot{Z}(t)$ is the friction force acting on the slider along the X-axis due to rigid body motion, m_4 represents the mass of the slider, δ is the foreshortening due the bending deflection of the rod, and the $\mu_s \dot{\delta}$ term represents the slider friction due to elastic deformation.

The rigid body piston acceleration $\ddot{Z}(t)$ is easily determined from the rigid body kinematic analysis. In order to retain the motion of the piston end along the X direction, we must have

$$L \sin(-\phi) = r \sin \omega t, \tag{8}$$

which can be written in the dimensionless form

$$\sin \phi = -\xi \sin \omega t, \tag{9}$$

where ξ represents the ratio of the crank throw to the length of the connecting rod and is specified as the length ratio. With this geometrical relation, the piston displacement function can be expressed as

$$Z(t) = r \cos \Omega t + L \cos \phi = L(\xi \cos \Omega t + \cos \phi), \tag{10}$$

from which $\dot{Z}(t)$ and $\ddot{Z}(t)$ are readily obtained.

The foreshortening along the x-axis due to the bending deflection of the connecting rod can be approximated to first order by assuming small transverse deformations:

$$\delta = \int_0^L \sqrt{1 + (\partial v / \partial x)^2} \, dx - L \approx \tfrac{1}{2} \int_0^L (\partial v / \partial x)^2 \, dx. \tag{11}$$

Substituting equation (5) into equation (2), we obtain

$$EI v_{xxxx} + \mu_c I v_{xxxxt} - [P(x, t) v_x]_x = \rho A \left[-r\omega^2 \sin(\omega t - \phi) + \frac{\partial^2 \phi}{\partial t^2} x + \frac{\partial^2 v}{\partial t^2} - \left(\frac{\partial \phi}{\partial t}\right)^2 v \right], \tag{12}$$

where $P(x, t)$ is given by equation (7), with $Z(t)$ and δ given in equations (10) and (11), respectively. Equation (12) describes the transverse motion of the connecting rod.

We now consider the boundary conditions for the connecting rod. Since the crank shaft is assumed to be perfectly rigid,

$$v(0, t) = 0. \tag{13}$$

Also, at $x = L$, the piston motion is constrained to move along the X-direction; thus,

$$v(L, t) = u(L, t) \tan(-\phi). \tag{14}$$

It can be shown that this boundary condition can be approximated by $v(L, t) = 0$ (see reference [15]). In addition, based on the simply supported assumption,

$$v_{xx}(0, t) = v_{xx}(L, t) = 0. \tag{15}$$

From these observations and assumptions, the solution $v(x, t)$ can be approximated as

$$v(x, t) = \sum_{n=1}^{N} \bar{v}_n(t) \sin(n\pi x/L), \tag{16}$$

where $\bar{v}_n(t)$ represents the contribution of the displacement at the mid-point of the beam due to the nth mode, and $\sin(n\pi x/L)$ are the natural modes of transverse vibration for a uniform beam with pinned ends. Previous work [4] has shown that higher order modes have insignificant influence on the transverse response of the connecting rod over the frequency range of most practical interest. Hence, it is assumed that the solution for $v(x, t)$ can be approximated by a single mode: $v(x, t) \approx \bar{v}_1(t) \sin(\pi x/L)$. Substituting this assumed solution into equation (12) and projecting the equation onto the first mode, we obtain, after rescaling,

$$(1 + \pi v \tan \phi + (S/2)\pi^4 v^2)\ddot{v} + 2\mu_2 \dot{v} + (2/\pi)(\ddot{\phi} - 2\xi\Omega^2 \sin(\Omega t - \phi))$$

$$+ v[1 + \ddot{\phi}\pi^2(S + \tfrac{1}{3})\tan \phi + \dot{\phi}^2(\pi^2/3 + \pi^2 S - \tfrac{5}{4}) + (\tfrac{1}{2} + S)\xi\Omega^2\pi^2 \cos \Omega t/\cos \phi]$$

$$+ 2v\mu_4(\dot{\phi} - \Omega)\pi^2 \tan \phi + v^2[\pi\ddot{\phi} + 2\pi\xi\Omega^2 \tan \phi \cos(\Omega t - \phi)] + 2\pi\dot{\phi}\dot{v}v \tan \phi$$

$$+ v^3((\pi^2/2)\ddot{\phi} \tan \phi) + (\pi^4/2)S\dot{v}^2v + v^2\dot{v}(\pi^2\dot{\phi} \tan \phi + \mu_4\pi^4) = 0, \tag{17}$$

where, for notational simplification, overdots represent derivatives with respect to non-dimensional time, $\bar{v}_1$ is replaced by v, and the following dimensionless parameters have been defined:

$$\bar{v} = v/L, \qquad \bar{x} = x/L, \qquad \xi = r/L, \qquad S = m_4/\rho AL, \qquad \omega_{1t}^2 = EI\pi^4/\rho AL^4,$$

$$\Omega = \omega/\omega_{1t}, \qquad \bar{t} = \omega_{1t}t, \qquad \mu_2 = \mu_c\omega_{1t}/2E, \qquad \mu_4 = \mu_s/2\rho AL\omega_{1t}.$$

We note that this equation contains the following features: (1) non-linear inertial terms; (2) external as well as parametric excitations arising from inertial forces; (3) dissipation effects; and (4) time-dependent quadratic and cubic non-linearities. Despite its complexities, each term of equation (17) has an identifiable physical source. All the terms involving the parameter S, except $((S/2)\pi^4 v^2\ddot{v})$ and $((S/2)\pi^4 v\dot{v}^2)$, which represent foreshortening effects, arise from the inertial force associated with the rigid body motion of the slider mass m_4. The forcing term $[(2/\pi)(\ddot{\phi} - 2\xi\Omega^2 \sin(\Omega t - \phi))]$ arises from the action of the transverse acceleration component a_y on the connecting rod. The following terms arise from the effects of the bending moments caused by the accelerations a_x and a_y: $\pi v\ddot{v} \tan \phi$, $(\ddot{\phi}/3)$ $\pi^2 v \tan \phi$, $v\dot{\phi}^2$, $(\epsilon/2)$ $\Omega^2\pi^2 v \cos \Omega t/\cos \phi$, $2\pi\xi\Omega^2 v^2 \tan \phi \cos(\Omega t - \phi)$, $(\pi^2/2)v^3\ddot{\phi} \tan \phi$ and $\pi^2 v^2\dot{v}\dot{\phi} \tan \phi$. All terms involving the parameter μ_4 arise from the friction force acting on the slider mass.

Now, let us reconsider equation (9). Since in most applications, the length ratio is smaller than one, equation (9) can be expanded in terms of the length ratio ξ to obtain

$$\phi = \sin^{-1}(\sin \Omega t)$$

$$= -(\xi \sin \Omega t) - (\xi \sin \Omega t)^3/6) - (\xi \sin \Omega t)^5/120 + \cdots$$

$$= -(\xi + 3\xi^2/4 + \cdots)\sin \Omega t - (3\xi^3/4 + \cdots)\sin 3\Omega t - (\xi^5/16 + \cdots)\sin 5\Omega t + \cdots. \tag{18}$$

This equation indicates that the excitation provided to the connecting rod is a superposition of harmonic inputs at frequencies which are multiples of the crank rotation speed. Also, note that the force amplitude associated with the nth harmonics is of order ξ^n.

3. ANALYSIS

3.1. METHOD OF MULTIPLE SCALES

Before applying the MMS (Method of Multiple Scales) to equation (17), first consider a solution to the linearized model of equation (17). To achieve this, the original equation of motion, equation (17), is expanded with the help of equations (9) and (18), and all first order terms in ξ, v and time derivatives of v are retained. This results in the equation

$$\ddot{v}(t) + 2\mu_2 \dot{v}(t) + v(t) = (2/\pi)\xi\Omega^2 \sin \Omega t, \tag{19}$$

which represents a linear oscillator subjected to an external excitation. The response of this equation is given by

$$v(t) = X \sin (\Omega t - \varphi), \tag{20}$$

where

$$X = (2/\pi)\, \xi\Omega^2 / \sqrt{(1 - \Omega^2)^2 + 4\mu_2^2\Omega^2} \tag{21}$$

and

$$\varphi = \tan^{-1} (2\mu_2\Omega/(1 - \Omega^2)). \tag{22}$$

Equation (20) represents the response of the linearized system for very small length ratios. From equation (21), it is seen that, to first order, the amplitude of the steady state response is proportional to the length ratio ξ as well as the square of the frequency ratio Ω. However, this estimate is not sufficient to capture the true response under certain resonance conditions. In the current section, the MMS [26] is used to locate these conditions and, in subsequent sections, the approximation of the response for each individual resonance condition is improved.

To apply MMS, a set of new independent time variables T_n is introduced, according to

$$T_n = \epsilon^n t. \tag{23}$$

It follows that the derivatives with respect to t become expansions in terms of the partial derivatives with respect to T_n, according to

$$\mathrm{d}/\mathrm{d}t = \partial/\partial T_0 + \epsilon\, \partial/\partial T_1 + \epsilon^2\, \partial/\partial T_2 + \cdots = D_0 + \epsilon D_1 + \epsilon^2 D_2 + \cdots, \tag{24}$$

$$\mathrm{d}^2/\mathrm{d}t^2 = D_0^2 + 2\epsilon D_0 D_1 + \epsilon^2 (D_1^2 + 2D_0 D_2) + \cdots, \tag{25}$$

where D_j denotes the partial derivative with respect to the independent time variable T_j. Moreover, it is initially assumed that the length ratio ξ can be ordered by $\xi = \epsilon\xi_1$. Since the amplitude of the response is, to leading order, proportional to the length ratio ξ, it is also assumed that the solution $v(t)$ can be represented by the expansion

$$v(t) = \epsilon v_1(T_0, T_1, T_2) + \epsilon^2 v_2(T_0, T_1, T_2) + \epsilon^3 v_3(T_0, T_1, T_2) + \cdots. \tag{26}$$

The damping parameters μ_2 and μ_4 are then rescaled in such a way that they show up in the final resonance condition, together with the detuning parameter, σ, which represents the nearness of the frequency ratio Ω to a resonance condition. Observations indicate that the scaling of μ_4 is assumed to be $O(1)$, and the order of μ_2 is the same as that of σ, the detuning parameter, which is assumed to be of $O(\epsilon^2)$. This leads to the following orderings of the damping coefficients in terms of ϵ: $\mu_2 = \epsilon^2\mu_{2_2}$ and $\mu_4 = \mu_{4_0}$. Substituting equations (23), (24) and (25) and the rescaled damping parameters into equation (17), and expanding and equating the coefficients of ϵ^j for $j = 1$ and 2, the following equations are obtained:

$$O(\epsilon):\quad D_0^2 v_1 + v_1 = (2/\pi)\epsilon_1\Omega^2 \sin \Omega T_0; \tag{27}$$

$$O(\epsilon^2):\quad D_0^2 v_2 + v_2 = -2D_0 D_1 v_1 - (S + \tfrac{1}{2})\xi_1\pi^2\Omega^2 v_1 \cos \Omega T_0 + (2/\pi)\Omega^2\xi_1^2 \sin 2\Omega T_0. \tag{28}$$

In obtaining the general solution of $v_1(T_0, T_1, T_2)$ from equation (27), we need to distinguish between the following special cases: (1) Ω is near to unity and (2) Ω is away from unity. The case in which Ω is near to one corresponds to the primary resonance. When this occurs, the linear estimate (equation (20)) fails to provide a good prediction of the response. This case will be investigated later so, for the present, let us assume that Ω is away from one and continue our analysis. Under this condition, the general solution of $v_1(T_0, T_1, T_2)$ is given as the combination of the homogeneous and particular solutions,

$$v_1(T_0, T_1, T_2) = A_1(T_1, T_2) \exp(jT_0) + \Lambda_4 \sin \Omega T_0 + c.c., \tag{29}$$

where A_1 is an unknown complex function which will be determined later, Λ_4 is given by

$$\Lambda_4 = (2/\pi)\xi_1 \Omega^2/(1 - \Omega^2), \tag{30}$$

and c.c. denotes the complex conjugate of the preceding terms on the right side of equation (29). Note that, according to the linear theory, the homogeneous part of solution (29), i.e., the $A_1 \exp(jT_0)$ term, will decay to zero due to the presence of the damping parameters. Thus, the homogeneous solution is not included in the steady state response of the linear system (equation (20)). For the present, the homogeneous solution is included in the solution, and we proceed to find the conditions for which this homogeneous solution does not decay to zero. The reason for the retention of the homogeneous solution will become clear. Substituting the solution $v_1(T_0, T_1, T_2)$ into equation (28), we obtain

$$\begin{aligned}
D_0^2 v_2 + v_2 = &-2j(D_1 A_1)\exp(jT_0) + (1/\pi)\xi_1^2 \Omega^2 \exp(2j\Omega T_0 - j\pi/2) \\
&-(S - \tfrac{1}{2})\xi_1 \Omega^2 \pi^2 (A_1/4) \exp(2j\Omega T_0 - j\pi/2) \\
&-(S + \tfrac{1}{2})\xi_1 \Omega^2 \pi^2 (A_1/2) \exp(j\Omega T_0 + jT_0) \\
&-(S + \tfrac{1}{2})\xi_1 \Omega^2 \pi^2 (A_1/2) \exp(j\Omega T_0 - jT_0) + c.c.
\end{aligned} \tag{31}$$

In analyzing the particular solution of equation (31), there are three cases which need to be considered separately; (1) Ω is near to $\tfrac{1}{2}$, (2) Ω is near to 2, and (3) Ω is not near $\tfrac{1}{2}$ or 2. The first case corresponds to a superharmonic resonance, while the second one corresponds to a subharmonic resonance, the principal parametric resonance. Both of these cases are considered in detail and improved approximations are provided in sections 3.4 and 3.2, respectively. For the present, it is assumed that Ω is away from $\tfrac{1}{2}$ and 2, and the analysis is continued. When Ω is not near $\tfrac{1}{2}$ or 2,

$$D_1 A_1(T_1, T_2) = 0 \tag{32}$$

must hold in order to remove the secular term from the particular solution of v_2. This implies that the unknown amplitude function $A_1(T_1, T_2)$ must be independent of the time variable T_1. As a consequence of this, all the higher order solutions are assumed to be independent of the time variable T_1. The particular solution of $v_2(T_0, T_2)$ is then given by

$$\begin{aligned}
v_2 = &\frac{1}{1 - 4\Omega^2}\left[\frac{\xi_1^2 \Omega^2}{\pi} - \left(\frac{S}{4} + \frac{1}{8}\right)\xi_1 \pi^2 \Omega^2 A_1\right]\exp\left(2j\Omega T_0 - j\frac{\pi}{2}\right) \\
&-\frac{1}{1 - (1 + \Omega)^2}\left(\frac{S}{2} + \frac{1}{4}\right)\xi_1 \Omega^2 \pi^2 A_1 \exp(j\Omega T_0 + jT_0) \\
&-\frac{1}{1 - (1 - \Omega)^2}\left(\frac{S}{2} + \frac{1}{4}\right)\xi_1 \Omega^2 \pi^2 \overline{A}_1 \exp(j\Omega T_0 - jT_0) + c.c.
\end{aligned} \tag{33}$$

At this point, a brief discussion of some of the general features of this analysis procedure is in order. By using the assumed solution sequence, the equations describing the transverse

vibration of the connecting rod can be transformed into a sequence of ordinary differential equations, which are solved relatively easily, since they are linearized by the nature of the perturbation expansion. In solving these sequential equations, several resonant conditions arise. The primary resonance arises first and then the principal parametric resonance. After these two resonances, several secondary resonances arise. In principle, it is possible to extend this analysis to study even higher order resonances, for instance, the subharmonic resonance which occurs when Ω is near $3\omega_n$. In fact, Hsieh [29] had extended the current method of analysis to consider all super- and subharmonic resonances up to order three. However, each higher order involves a non-trivial increase in the required amount of computational work.

Although the primary resonance arises first in the above procedure, in the analysis below, the principle parametric resonance is considered first, followed by an investigation of the primary resonance, since this simplifies the analysis somewhat. After these two cases, the superhamonic resonance of order two is investigated.

3.2. PRINCIPAL PARAMETRIC RESONANCE ($\Omega \approx 2$)

In analyzing the particular solution of equation (31), when the frequency ratio Ω is near to 2, a principle parametric resonance takes place. To describe the dynamics when the frequency ratio is close to 2, Ω is expressed as

$$\Omega = 2 + 2\epsilon\sigma_1, \tag{34}$$

where σ_1 is the detuning parameter. The damping parameter μ_4 is reordered by $\mu_4 = \mu_{4_0}$. Moreover, the damping parameter μ_2 is rescaled according to $\mu_2 = \epsilon\mu_{2_1}$ so that it will appear, together with detuning parameter σ_1, in the final resonant condition. After carrying out the same procedure as that described in the last section, equation (28) reduces to

$$D_0^2 v_2 + v_2 = -2j(D_1 A_1) \exp(jT_0) - 2j\mu_{2_1} A_1 \exp(jT_0)$$
$$-(S/2 + \tfrac{1}{4})\xi_1 \Omega^2 \pi^2 \bar{A}_1 \exp(jT_1 + 2j\sigma_1 T_0)$$
$$-\xi_1 \Omega \pi^2 \mu_{4_0} \bar{A}_1 \exp(2j\sigma_1 T_1 - j\pi/2) + N.S.T. + c.c., \tag{35}$$

where $N.S.T.$ represents those terms which will not produce secular terms in the particular solution of $v_2(T_0, T_1, T_2)$. In order to eliminate the secular terms, the following must hold:

$$-2j(D_1 A_1) - 2j\mu_{2_1} A_1 - 4(S/2 + \tfrac{1}{4})\xi_1 \pi^2 \bar{A}_1 \exp(2j\sigma_1 T_0)$$
$$-2\pi^2 \mu_{4_0} \xi_1 \bar{A}_1 \exp(2j\sigma_1 T_1 - j\pi/2) = 0. \tag{36}$$

Expanding equation (36) with $A_1 = (a/2) \exp(j\Psi)$, and separating the resultant equation into real and imaginary parts, the following differential equations which govern a and Φ are obtained:

$$a' = -\mu_{2_1} a - 2a\xi_1 \Delta_4 \sin 2\Phi_1 + a\pi^2 \mu_{4_0} \xi_1 \cos 2\Phi_1, \tag{37}$$

$$a\Phi_1' = \sigma_1 a - 2a\xi_1 \Delta_4 \cos 2\Phi_1 - a\pi^2 \mu_{4_0} \xi_1 \sin 2\Phi_1, \tag{38}$$

where

$$\Phi_1 = \sigma_1 T_1 - \Psi, \qquad \Delta_4 = (2S + 1)(\pi^2/4), \tag{39, 40}$$

and the primes indicate derivatives with respect to T_1. The steady state response conditions are obtained by letting $a' = 0$ and $\Phi_1' = 0$. This yields

$$\mu_{2_1} a = -2a\xi_1 \Delta_4 \sin 2\Phi_1 + a\pi^2 \xi_1 \mu_{4_0} \cos 2\Phi_1, \tag{41}$$

$$\sigma_1 a = 2a\xi_1 \Delta_4 \cos 2\Phi_1 + a\pi^2 \xi_1 \mu_{4_0} \sin 2\Phi_1. \tag{42}$$

Squaring these equations, and adding them together results in

$$[\sigma_1^2 + \mu_{2_1}^2 - (2\xi_1\varDelta_4)^2 - (\pi^2\xi_1\mu_{4_0})^2]a^2 = 0. \tag{43}$$

Equation (43) is an equation which can be solved for the amplitude a as a function of the detuning parameter, the damping parameters and the length ratio. From this equation, it is seen that the trivial solution $a = 0$ is the unique steady state response for the current resonant condition. To determine the stability of this solution, we substitute $A_1 = (B_R + jB_I)\exp(j\sigma_1 T_1 + \gamma T_1)$ into equation (36), in which B_R and B_I are two real constants, and separate the resultant equations into real and imaginary parts to obtain two equations. The non-trivial constant solutions of B_R and B_I are obtained from these two equations [26]. From this, it is determined that the trivial solution is unstable when

$$\sigma_1^2 + \mu_{2_1}^2 < \xi_1^2(4\varDelta_4^2 + \pi^4\mu_{4_0}^2) \tag{44}$$

is satisfied. The curve given by $\sigma_1^2 + \mu_{2_1}^2 = \xi_1^2(4\varDelta_4^2 + \pi^4\mu_{4_0}^2)$ represents the transition curve along which one of the eigenvalues associated with a and Φ are either $+1$ or -1. In the unstable region, any disturbance, no matter how small, applied to the steady state response results in unbounded growth in the response amplitude of the linear model. In the remaining part of this section, the analysis is extended to investigate the non-linear effects which then dictate the response.

In order to capture the effects of the non-linearities, it is necessary to reorder either the solution or the parameters, so that the non-linearities will be included in the equation describing the resonant condition. For the present problem, the amplitude of the response is proportional to the length ratio (equation (21)). Therefore, a reordering of the length ratio is equivalent to a reordering of the solution. To carry out the non-linear analysis, the length ratio ξ is reordered according to $\xi = \epsilon^2\xi_2$. Moreover, the damping parameters μ_2 and μ_4 are rescaled as $\mu_2 = \epsilon^2\mu_{2_2}$ and $\mu_4 = \mu_{4_0}$. Expanding equation (17) with these rescaled relations, and equating the coefficients of ϵ^j for $j = 1$, 2 and 3, the following equations are obtained:

$$O(\epsilon): \quad D_0^2 v_1 + v_1 = 0; \tag{45}$$

$$O(\epsilon^2): \quad D_0^2 v_2 + v_2 = -2D_0 D_1 v_1 + \left(\frac{2}{\pi}\right)\xi_2\Omega^2 \sin\Omega T_0; \tag{46}$$

$$O(\epsilon^3): \quad D_0^2 v_3 + v_3 = -2D_0 D_2 v_1 - 2\mu_{2_2} D_0 v_1 - \pi^4 S(D_0^2 v_1^3) - 2\mu_{4_0}\pi^2\xi_2\Omega v_1 \sin\Omega T_0$$
$$- D_1^2 v_1 - 2D_0 D_1 v_2 - \pi^2(S + \tfrac{1}{2})\xi_2\Omega^2 v_1 \cos\Omega T_0 - \pi^4\mu_{4_0}(D_0 v_1)v_1^2. \tag{47}$$

Equation (45) admits the solution

$$v_1(T_0, T_1, T_2) = A(T_1, T_2)\exp(jT_0) + c.c. \tag{48}$$

Substituting this solution into equation (46) yields

$$D_0^2 v_2 + v_2 = -2j(D_1 A_1)\exp(jT_0) + (2/\pi)\xi_2\Omega^2 \sin\Omega T_0 + c.c. \tag{49}$$

In analyzing the solution of this equation, one needs to distinguish between two cases: (1) Ω is near to one and (2) Ω is away from one. At this moment, case (2) is of interest. When Ω is away from one, $D_1 A_1 = 0$, which implies the independence of A_1 with respect to the

time variable T_1. Therefore, all higher order solutions are also assumed to be independent of T_1. With this assumption, equation (47) reduces to

$$D_0^2 v_3 + v_3 = -2j\mu_{2_2} A_1 \exp(jT_0) - 2j(D_1 A_1)\exp(jT_0) - j\mu_{4_0}\pi^4 A_1^2 \bar{A}_1 \exp(jT_0)$$
$$-(S + \tfrac{1}{2})\xi_2 \Omega^2 \pi^2 (\bar{A}_1/2)\exp(j\Omega T_0 - jT_0) - 2\mu_{4_0}\pi^2 \xi_2 \bar{A}_1 \exp(j\Omega T_0 - j\pi/2)$$
$$+\pi^4 S A_1^2 \bar{A}_1 \exp(jT_0) + N.S.T. + c.c., \tag{50}$$

which describes the third order term in the flexural response associated with the connecting rod. To describe the nearness of Ω to 2, Ω is expressed as

$$\Omega = 2 + 2\epsilon^2 \sigma_2. \tag{51}$$

Hence, we must have

$$-2j\mu_{2_2} A_1 - 2j(D_2 A_1) - 4\xi_2 \Delta_4 \bar{A}_1 \exp(2j\sigma_2 T_2) + \pi^4 A_1^2 \bar{A}_1 (S - j\mu_{4_0})$$
$$-2\mu_{4_0}\pi^2 \xi_2 \bar{A}_1 \exp(2j\sigma_2 T_2 - j\pi/2) = 0 \tag{52}$$

in order to remove the secular terms from the particular solution of v_1. Substituting $A_1 = (a/2)\exp(j\Psi)$ into equation (52) and separating the resultant equation into real and imaginary parts results in

$$a' = -\mu_{2_2} a - \mu_{4_0}\pi^4 a^3/8 - 2\xi_2 \Delta_4 a \sin 2\Phi_2 + \xi_2 \pi^2 \mu_{4_0} a \cos 2\Phi_2, \tag{53}$$

$$a\Phi_2' = \sigma_2 a - 2\xi_2 \Delta_4 a \cos 2\Phi_2 - \xi_2 \pi^2 \mu_{4_0} a \sin 2\Phi_2 + \Delta_5 a^3, \tag{54}$$

where Φ_2 and Δ_5 are defined by

$$\Phi_2 = \sigma_2 T_2 - \Psi, \qquad \Delta_5 = \tfrac{1}{8}\pi^4 S, \tag{55, 56}$$

and primes represent derivatives with respect to the time scale T_2. The frequency response equation then takes the form

$$a^2[(\mu_{2_2} + \mu_{4_0}\pi^4 a^2/8)^2 + (\sigma_2 + \Delta_5 a^2)^2 - (2\xi_2 \Delta_4)^2 - (\pi^2 \xi_2 \mu_{4_0})^2] = 0. \tag{57}$$

From this equation, the non-trivial solutions of a^2 are

$$(a_2)^2 = (1/k)[-l + \sqrt{l^2 - km}], \qquad (a_3)^2 = (1/k)[-l - \sqrt{l^2 - km}], \tag{58, 59}$$

where

$$k = [\tfrac{1}{8}\mu_{4_0}\pi^4]^2 + \Delta_5^2, \qquad l = \tfrac{1}{8}\mu_{4_0}\mu_{2_2}\pi^4 + \Delta_5 \sigma_2, \tag{60, 61}$$

$$m = \mu_{2_2}^2 + \sigma_2^2 - (2\xi_2 \Delta_4)^2 - (\pi^2 \xi_2 \mu_{4_0})^2. \tag{62}$$

From equations (58) and (59), it is seen that a_2 and a_3 exist only when

$$l^2 - km > 0. \tag{63}$$

This implies that the magnitude of the forcing term must be above a certain critical level in order to produce a sustained non-trivial steady state response. In particular, the following condition

$$\sigma_2 < \sqrt{(2\xi_2 \Delta_4)^2 + (\pi^2 \xi_2 \mu_{4_0})^2 - \mu_{2_2}^2} \tag{64}$$

is required for the existence of a_2, and

$$\sigma_2 < -\sqrt{(2\xi_2 \Delta_4)^2 + (\pi^2 \xi_2 \mu_{4_0})^2 - \mu_{2_2}^2} \tag{65}$$

is required for the existence of a_3. In order to determine the stability of these steady state responses the Jacobian matrix associated with equations (53) and (54) is computed from which the following conclusions are obtained: (1) when $\sigma_2 > \sqrt{(2\xi_2 \Delta_4)^2 + (\pi^2 \xi_2 \mu_{4_0})^2 - \mu_{2_2}^2}$, only the trivial solution is possible, and it is stable; (2) when $|\sigma_2| <$

$\sqrt{(2\xi_2 \Delta_4)^2 + (\pi^2 \xi_2 \mu_{4_0})^2 - \mu_{2_2}^2}$, the trivial solution becomes unstable, while a_2 exists and is stable, and a_3 does not exist; (3) when $\sigma_2 < -\sqrt{(2\xi_2 \Delta_4)^2 + (\pi^2 \xi_2 \mu_{4_0})^2 - \mu_{2_2}^2}$, a_3 exists and is unstable, and a_2 and a_1 exist and are stable.

Before leaving this section, a few points need to be made. First, compare the linear resonance condition (equations (37) and (38)) with the non-linear version (equations (53) and (54)). They are identical at linear order. The difference in the equations describing the variation of the amplitude, a, is the non-linear term $\frac{1}{8}\mu_{4_0}a^3$. This term arises from the slider friction induced by elastic deformation. The difference in the equations describing the variation of phase angle, Φ_2, is the $\Delta_5 a^3$ term in equation (54), which arises from the slider inertia. The frequency response equations obtained from the linear and non-linear analyses coincide at linear order, and the influence of the non-linearity can be determined by a direct comparison. In the absence of the non-linearity, the response is globally unstable when the parameters are located inside the unstable region. Due to non-linear effects, however, an increasing response amplitude will be accompanied with an increase of the resistance force and a change of the phase angle Φ. The resistance force arises from the foreshortening introduced by elastic deformation. As the amplitude of the response increases, this resistance force, the magnitude of which is proportional to the foreshortening, also increases. The amplitude of response reaches a dynamic equilibrium state when this resistance offsets the effect of the slider friction introduced by the rigid body motion.

3.3. PRIMARY RESONANCE ($\Omega \approx 1$)

In order to bring out the effects of the non-linearities near primary resonance, it can be shown that the following scalings are required [29]: $\xi = \epsilon^3 \xi_3$, $\mu_4 = \mu_{4_0}$, $\mu_2 = \epsilon^2 \mu_{2_2}$ and $\Omega = 1 + \epsilon^2 \sigma_2$. Substituting this reordering relation into equation (17), expanding and equating the coefficients of ϵ^j, a new sequence of equations is obtained. The procedure of section 3.2 yields the following condition for removal of the secular terms from the particular solutions of v_3:

$$-2j(D_2 A_1) - 2j\mu_{2_2} A_1 - j\mu_{4_0}\pi^4 A_1^2 \bar{A}_1 + (1/\pi)\xi_3 \Omega^2 \exp{(j\sigma_2 T_2 - j\pi/2)} + \pi^4 A_1^2 \bar{A}_1 = 0. \quad (66)$$

Expanding equation (66) with $A_1 = (a/2)\exp{(j\Psi)}$, and separating the resulting equation into real and imaginary parts, gives

$$a' = -\mu_{2_2} a - \mu_{4_0} \pi^4 a^3/8 - (\xi_3/\pi)\cos{\Phi_2}, \qquad a\Phi_2' = \sigma_2 a + \Delta_5 a^3 + (\xi_3/\pi)\sin{\Phi_2}, \quad (67, 68)$$

where Φ_2 is given in equation (55) and Δ_5 is given in equation (56). The solution $v(t)$ can be approximated by

$$v(t) = \epsilon v_1(T_0, T_1, T_2) + O(\epsilon^2) = \epsilon a \cos{(\Omega T_0 - \Phi)} + O(\epsilon^2), \quad (69)$$

where a and Φ are described by equations (67) and (68).

The frequency response equation is then given by

$$a^2[(\mu_{2_2} + \mu_{4_0}\pi^4 a^2/8)^2 + (\sigma_2 + \Delta_5 a^2)^2] = (\xi_3/\pi)^2. \quad (70)$$

Equations (70) admits a peak amplitude, a_p, which is determined by solving

$$(\xi_3/\pi)^2 - a_p^2[\mu_{2_2} + \frac{1}{8}\mu_{4_0}\pi^4 a_p^2]^2 = 0. \quad (71)$$

Moreover, this maximum amplitude occurs at the frequency $\Omega = 1 + \epsilon^2 \sigma_{2_p}$, where

$$\sigma_{2_p} = -\Delta_5 a_p^2. \quad (72)$$

The negative sign in equation (72) implies that the response curve reaches this peak amplitude at a frequency of less than one. Thus, the frequency response curve bends to

the left, corresponding to a softening type of non-linearity. Hence, over a region of Ω values below one, there will generally exist more than one steady state response.

The stability of the steady state responses can be determined by computing the eigenvalues of the Jacobian matrix associated with equations (67) and (68). From the eigenvalues associated with this Jacobian matrix, it is determined that when

$$[\mu_{2_2} + \tfrac{1}{8}\mu_{4_0}\pi^4 a^2][\mu_{2_2} + \tfrac{3}{8}\mu_{4_0}\pi^4 a^2] + (\sigma_2 + \Delta_5 a^2)(\sigma_2 + 3\Delta_5 a^2) < 0, \tag{73}$$

the steady state responses are unstable. Otherwise, they are stable.

Before closing this section, a few points should be mentioned. First, consider neglecting the effects of μ_{4_0}, and compare the final equations describing the resonant conditions from the linear and the non-linear analyses. A prudent observation shows that the maximum amplitude of the response obtained from the linear (equation (21)) and non-linear analyses (equation (71)) are exactly the same for $\mu_{4_0} = 0$. This implies that linear theory is sufficient to provide a good approximation of the peak amplitude of the steady state response. However, if one compares the frequency at which the steady state response of the system reaches its maximum amplitude, there exists a difference between the results from the linear and non-linear analyses. Linear analysis indicates that this peak amplitude is observed at $\Omega = 1$, while the non-linear analysis show that the response achieves this amplitude when Ω is at $\Omega_p = 1 - \Delta_5 a_p^2$.

Finally, consider the effects of μ_{4_0}, which represents slider friction. According the analysis, μ_{4_0} has a favorable effect in reducing the amplitude of the response. This is caused by the foreshortening accompanied with the transverse deformation of the connecting rod. The existence of the slider friction will resist further deformation and hence has a tendency in reducing the amplitude of the response. (This is true only at leading order, and it is obvious that very large friction would lead to large amplitudes.)

3.4. SUPERHARMONIC RESONANCE ($\Omega \approx \tfrac{1}{2}$)

In analyzing the particular solution of v_2 from equation (31), it is assumed that Ω is away from 2 and $\tfrac{1}{2}$. When Ω is near to $\tfrac{1}{2}$, a superharmonic resonance occurs. For Ω near to $\tfrac{1}{2}$, the frequency ratio Ω is conveniently expressed as

$$\Omega = \tfrac{1}{2}(1 + \epsilon\sigma_1). \tag{74}$$

In addition, the damping parameter μ_2 is rescaled according to $\mu_2 = \epsilon\mu_{2_1}$ so that it appears with the detuning parameter σ_1 in the final resonant condition. Following the procedure of sections 3.2 and 3.3, the following resonant condition is obtained:

$$(\mu_{4_0}/6)\xi_1^2\pi \exp(j\sigma_1 T_1) - 2j(D_1 A_1) - 2j\mu_{2_1}A_1 + (\xi_1^2/12\pi)(3 - \Delta_4)\exp(j\sigma_1 T_1 - j\pi/2) = 0, \tag{75}$$

from the elimination of the secular terms of the particular solution of the resultant equation. Here, σ_1 is given in equation (74) and Δ_4 is defined by equation (40). Therefore, when Ω is near to $\tfrac{1}{2}$, the response equation takes the form

$$v(t) = \epsilon v_1(T_0, T_1, T_2) + O(\epsilon^2) = \epsilon[\Delta_4 \sin \Omega T_0 + a_s \cos(2\Omega T_0 - \Phi_s)] + O(\epsilon^2), \tag{76}$$

where Δ_4 is given in equation (30). The steady state value of the phase angle Φ_s is given by

$$\Phi_s = \tan^{-1}\left[\frac{\sigma_1(3 - \Delta_4) - 2\pi^2\mu_{2_1}\mu_{4_0}}{2\pi^2\sigma_1\mu_{4_0} + (3 - \Delta_4)\mu_{2_1}}\right] \tag{77}$$

and the amplitude of the steady state response a_s is described by

$$(\mu_{2_1}^2 + \sigma_1^2)a_s^2 = \xi_1^4[(\mu_{4_0}\pi/6)^2 + ((3 - \Delta_4)/12\pi)^2]. \tag{78}$$

TABLE 1

Identification of combinations of parameters

Case	ζ	S	μ_2	μ_3	μ_4	Case	ζ	S	μ_2	μ_3	μ_4
1	0·005	0·00	0·02	0·00	0·00	2	0·005	0·50	0·02	0·00	0·00
3	0·005	1·00	0·02	0·00	0·00	4	0·010	0·00	0·02	0·00	0·00
5	0·010	0·50	0·02	0·00	0·00	6	0·010	1·00	0·02	0·00	0·00
7	0·050	0·00	0·02	0·00	0·00	8	0·050	0·50	0·02	0·00	0·00
9	0·050	1·00	0·02	0·00	0·00	10	0·050	0·50	0·04	0·00	0·00
11	0·010	1·00	0·02	0·00	0·40	12	0·050	0·00	0·02	0·00	0·40

Equation (78) represents the steady state frequency response near this superharmonic resonance, and equation (76) represents the first order approximation of the response. Note that v_1 consists of two parts; the first term is the particular solution and the second term is from free oscillation. Hence, the homogeneous solution does not generally decay to zero; this is caused by the last term on the right side of equation (28). The amplitude of the particular solution is proportional to the length ratio ζ, while the second term is proportional to ζ^2. This implies that the second term vanishes more rapidly than the first as the length ratio ζ is decreased. A simple calculation of the eigenvalues of the Jacobian matrix shows that this homogeneous solution is stable everywhere for $\mu_{2_1} > 0$. Hence, a steady state superharmonic resonance exists for $\mu_{2_1} > 0$, and the response is composed of two terms with different frequencies. The particular solution possesses the same frequency as that of the external excitation, while the homogeneous solution oscillates with twice the frequency of the external excitation. It should be noted that this result is simply an expansion of the response of the *linearized* time-varying system in terms of ζ, with the second harmonic term arising from the 2Ω term in the excitation.

Near this resonance, an interesting observation is made regarding the influence of the mass ratio S on the amplitude of the homogeneous solution. The amplitude of the homogeneous solution is described by equation (78), and this can be minimized. It is determined that a_s reaches a minimum value when $\Delta_4 = 3$. This implies that a proper choice of the mass ratio can be used to suppress this superharmonic resonance. The existence of the slider friction, $\mu_4 \neq 0$, prevents the homogeneous solution from having a zero amplitude. This indicates that the damping parameter μ_{4_0} has an adverse effect on the response of the system for this superharmonic resonance.
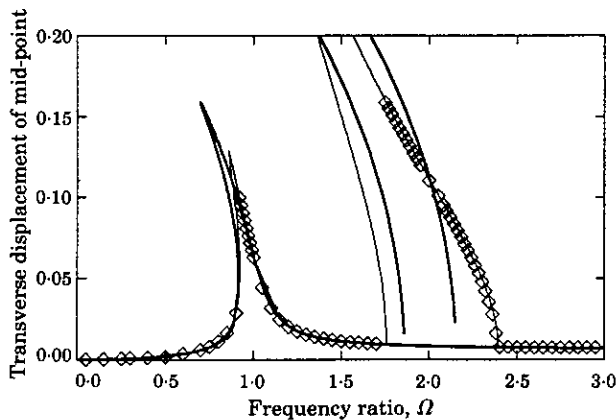

Figure 2. Frequency response curves from MMS ——, AUTO (————) and LSODE ($\diamond$) for $\zeta = 0·01$, $S = 0·50$, $\mu_2 = 0·02$ and $\mu_4 = 0·00$.

TABLE 2

Comparison of bifurcation data

Case	Analytical		AUTO	
1	$PD_1 = 1.9855$	$PD_2 = 2.0145$	$PD_1 = 1.9700$	$PD_2 = 2.0330$
2	$LP_1 = 0.9711$	$LP_2 = 0.999$	$LP_1 = -$	$LP_2 = -$
	$PD_1 = 1.9549$	$PD_2 = 2.0451$	$PD_1 = 1.9131$	$PD_2 = 2.1013$
3	$LP_1 = 0.9270$	$LP_2 = 0.9643$	$LP_1 = 0.9505$	$LP_2 = 0.9390$
	$PD_1 = 1.9287$	$PD_2 = 2.0713$	$PD_1 = 1.8680$	$PD_2 = 2.1670$
4	$PD_1 = 1.9549$	$PD_2 = 2.0450$	$PD_1 = 1.9153$	$PD_2 = 2.0996$
5	$LP_1 = 0.8477$	$LP_2 = 0.9296$	$LP_1 = 0.9353$	$LP_2 = 0.9104$
	$PD_1 = 1.9034$	$PD_2 = 2.0966$	$PD_1 = 1.8290$	$PD_2 = 2.2312$
6	$LP_1 = 0.6925$	$LP_2 = 0.9092$	$LP_1 = 0.8582$	$LP_2 = 0.9215$
	$PD_1 = 1.8533$	$PD_2 = 2.1467$	$PD_1 = 1.7564$	$PD_2 = 2.3909$
7	$PD_1 = 1.7541$	$PD_2 = 2.2459$	$PD_1 = 1.6354$	$PD_2 = 2.8600$
8	$LP_1 = 0.7830$	$LP_2 = -2.8534$	$LP_1 = 0.8430$	$LP_2 = 0.7003$
	$PD_1 = 1.5067$	$PD_2 = 2.4931$	$PD_1 = 1.3593$	$PD_2 > 3.00$
9	$LP_1 = -$	$LP_2 = -$	$LP_1 = 0.8133$	$LP_2 = 0.5956$
	$PD_1 = 1.2600$	$PD_2 = 2.7400$	$PD_1 = 1.0936$	$PD_2 > 3.00$
10	$LP_1 = 0.7873$	$LP_2 = -$	$LP_1 = 0.8473$	$LP_2 = 0.7799$
	$PD_1 = 1.5081$	$PD_2 = 2.4919$	$PD_1 = 1.3625$	$PD_2 > 3.0$
11	$LP_1 = 0.6925$	$LP_2 = -$	$LP_1 = 0.8612$	$LP_2 = 0.9202$
	$PD_1 = 1.8531$	$PD_2 = 2.1469$	$PD_1 = 1.7481$	$PD_2 = 2.4045$
12	$PD_1 = 1.7509$	$PD_2 = 2.2491$	$PD_1 = 1.5537$	$PD_2 = -$

4. DISCUSSION AND NUMERICAL SOLUTIONS

In the present section, a numerical simulation study of equation (17) is presented, the main purpose of which is to explore the effects of the system parameters on the resonances and to verify the analytical results. A systematic approach is adopted in which specific sets of parameter values are considered; these cases are given in Table 1. In obtaining the numerical solutions, the software packages LSODE [27] and AUTO [28] were used. The former is a numerical solution package for solving initial values problems for ordinary differential equations, and the latter is a software package capable of tracking steady state response curves and providing stability information. AUTO is used to obtain response curves over a large range of Ω values and LSODE is used to provide time traces for specific parameter values.

The general features of the response of the system modelled by equation (17) are demonstrated in Figure 2. The analytically predicted frequency response curve is compared with that computed by AUTO and with simulations from LSODE at several frequencies for a specific set of parameter values. From this figure, it is seen that the important features of the response are captured by the MMS analysis for small values of the length ratio. In particular, the bending of the primary resonance near $\Omega = 1$ and the parametric resonance near $\Omega = 2$ appear in the simulations and in both response curves. However, when the
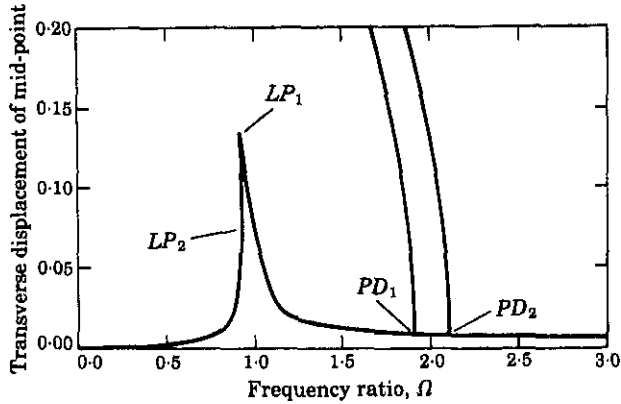
Figure 3. Location of points PD_1, PD_2, LP_1 and LP_2.

length ratio ξ is larger than 0·10, the analytical results provide only rough qualitative consistency with the actual results.

Table 2 contains bifurcation information obtained from analytical results and AUTO. In this table, PD_1 and PD_2 indicate the points at which principal parametric resonance instabilities occur, while the turning points associated with the primary resonance are marked by LP_1 and LP_2. (This notation is from AUTO, since period-doubling birfurcations occur at PD points, and limit-point, or saddle-node, bifurcations occur at LP points.) The locations of these points are indicated in Figure 3. The region between points PD_1 and PD_2 represents the main region of instability near $\Omega = 2$, and the region between points LP_1 and LP_2 represents the range of multiple steady states near $\Omega = 1$. For the sake of clearness in the figures, the branches of the non-trivial response associated with the parametric resonance are often not included.

The effects of the system parameters on the overall response are now considered. In section 4.1, the effect of the length ratio ξ on the response is described. In section 4.2, the effect of the mass ratio S on the response is considered. The effects of the damping parameters μ_2 and μ_4 are examined in sections 4.3 and 4.4, respectively. In section 4.5, the influence of the frequency ratio Ω is described. For the sake of brevity, only certain key results are discussed. More detailed numerical studies and in-depth discussions can be found in Hsieh [29].
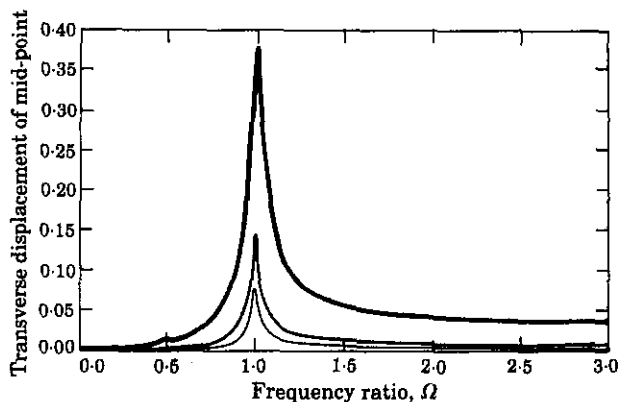
Figure 4. Frequency response for $S = 0$, $\mu_2 = 0·02$, $\mu_4 = 0$. ——, $\xi = 0·005$; ——, $\xi = 0·01$; ——, $\xi = 0·05$.
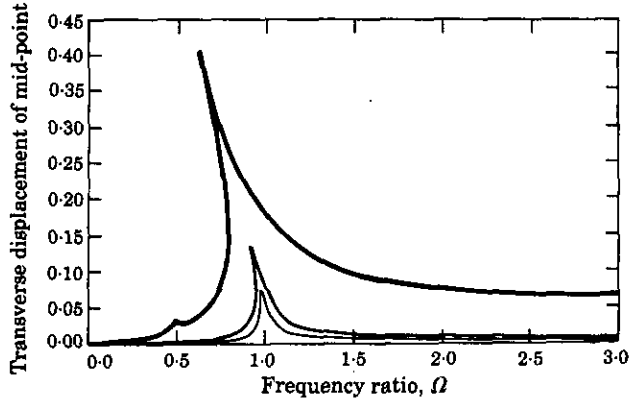
Figure 5. Frequency response for $S = 0.5$, $\mu_2 = 0.02$, $\mu_4 = 0$. ——, $\xi = 0.005$; ——, $\xi = 0.01$; ——, $\xi = 0.05$.

4.1. EFFECT OF THE LENGTH RATIO ξ

The length ratio ξ can be treated as the strength of the external excitation. This connecting rod is essentially a simply supported beam, subjected to both vertical and horizontal excitations arising from the same source: the motion of the crank and the kinematic constraints. The magnitude of this excitation is proportional to the length ratio ξ. An increase in ξ implies an increase in the inertial forces, and hence the magnitude of the excitation will increase.

The main effects of ξ are as follows: (1) the amplitude of response near the primary resonance is proportional to ξ, and this amplitude can be obtained using linear theory; (2) the width of the region of parametric instability grows as ξ is increased; (3) superharmonic resonances appear at $1/n$ as ξ increases, starting with the $\frac{1}{2}$ superharmonic, and the added amplitude near this resonance is proportional to ξ^n.

Frequency response curves for $S = 0.0$ with different ξ values (cases 1, 4 and 7) are shown in Figure 4. According to the analytical results, $S = 0$ corresponds to a linear oscillator, and hence there is no detuning associated with the primary resonance. Moreover, the amplitude of the response is proportional to ξ. The main region of instability exists near $\Omega = 2$. Both of these points are verified by Figure 4 and the bifurcation data shown in Table 2. Also, note that the superharmonic resonance near $\Omega = \frac{1}{2}$ just begins to appear as ξ is increased.
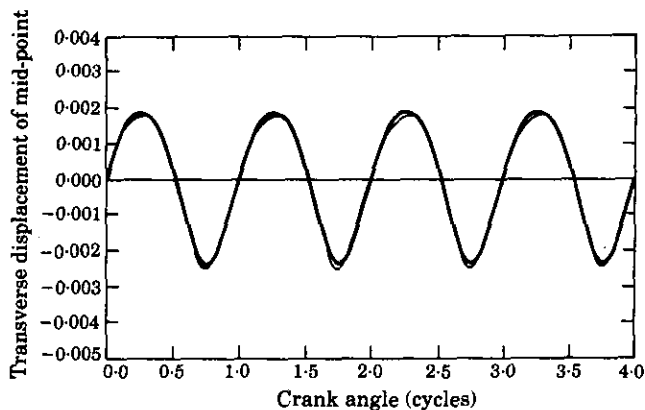

Figure 6. Comparison between simulation and analytical approximation for case 5 at $\Omega = 0.50$. ——, LSODE; ——, analytical.
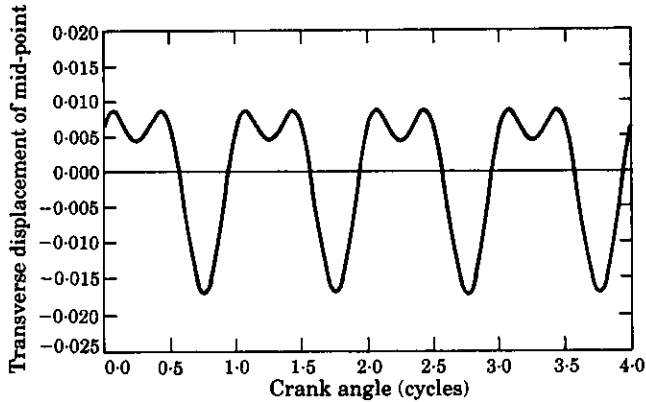
Figure 7. Comparison between simulation and analytical approximation for case 8 at $\Omega = 0.50$. ——, LSODE; ——, analytical.

Next, a case in which $S \neq 0$ is considered. According to the results from MMS, for $S > 0$, the systems possesses a softening type of non-linearity. The peak amplitude of the response is the same as that given in the linear approximation, while the detuning associated with the primary resonance (σ_p) is proportional to ξ^2. The numerical results for three ξ values with $S = 0.50$ are shown in Figure 5. Again, as ξ increases, the superharmonic resonance near $\Omega \approx \frac{1}{2}$ begins to appear. This is as predicted by the analysis of section 3.4.

Comparisons between the MMS approximations and simulation results for time traces at the superharmonic resonance ($\Omega = 0.5$) are shown in Figures 6 and 7. It is very clear that the MMS approximations match the simulation results almost exactly, and that the second harmonic is more prominent for larger values of ξ (Figure 7).

4.2. EFFECT OF THE MASS RATIO S

The main effects of S, which represents the primary source of non-linearity in the system, are as follows: (1) increases in S shift the peak amplitude of the primary resonance to the left, but have virtually no effect on the peak amplitude; (2) increases in S widen the region of parametric instability while lowering the vibration amplitude in the resonant region; (3) S has a varying effect on the superharmonic resonance near $\frac{1}{2}$, which may be used to suppress vibration amplitude near this resonance.
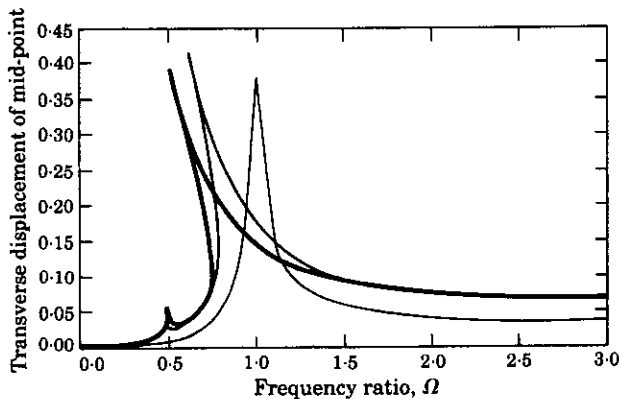

Figure 8. Frequency response curves from AUTO. ——, Case 7; ——, case 8; ——, case 9.
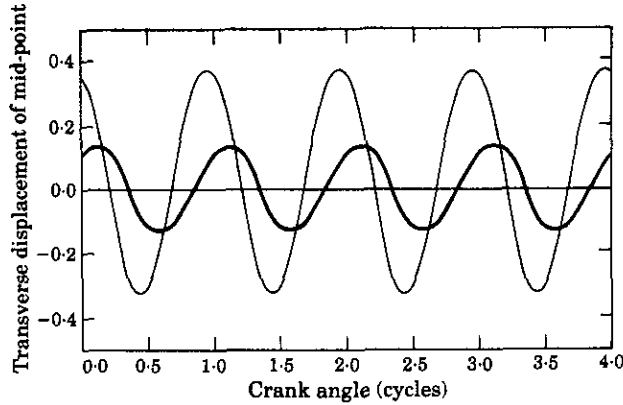
Figure 9. Simulation results from LSODE at $\Omega = 1.00$. ——, Case 7; ——, case 8.

The frequency response curves associated with cases 7, 8 and 9 are shown in Figure 8. First, consider the primary resonance. This figure shows that the detuning σ_p increases as S increases from zero to one. According to the analysis, the detuning associated with the primary resonance is directly proportional to S, while the peak amplitude remains unchanged. An increase in S also enlarges the instability region associated with the primary resonance. From the numerical results listed in Table 2, it is seen that the width of the instability region near $\Omega = 1$ increases from zero (case 4) to 0·0633 (case 6) as S increases from zero to one. The simulation results for cases 7 and 8 with $\Omega = 1.00$ are depicted in Figure 9. From this figure, it is observed that smaller peak response amplitudes occur at $\Omega = 1$ if S is increased. This is caused by the bending of the frequency response curves associated with the primary resonance (see Figure 8).

In the principal parametric resonance, the influence of S is included in the terms Δ_4 and Δ_5. According to the linear analysis, the main region of instability, i.e., the unstable region in the ξ–Ω plane, will be enlarged if the value of S is increased. To show this point, consider equations (58) to (65). From these equations, the following facts are determined: (1) the width of the unstable region increases as the mass ratio increases; (2) the amplitude of the non-trivial solutions a_2 and a_3 decreases as the mass ratio increases. With these two observations, it is seen that this parameter has both favorable and adverse effects on the principal parametric resonance. An increment of S will enlarge the unstable region, while this increment also reduces the amplitude of the non-trivial solutions. The physical reason
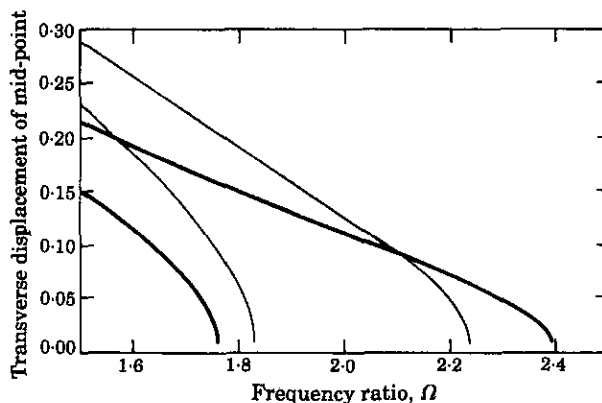

Figure 10. Non-trivial responses associated with the principal parametric resonance. ——, case 5; ——, case 6.
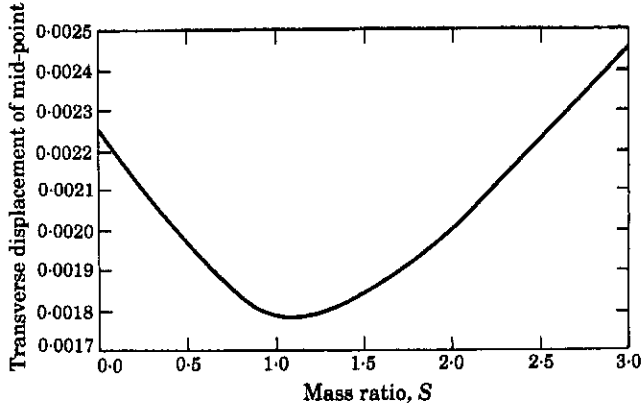
Figure 11. Amplitude of response at $\Omega = 0.50$ for $\zeta = 0.01$, $\mu_2 = 0.02$ and $\mu_4 = 0$.

for these features is the following: the slider mass provides a periodic inertial end load which helps destabilize the system in the usual way when Ω is near 2. However, once unstable, the motion is then limited by the same inertial resistance through foreshortening effects. As a numerical example, consider the width of the region of instability, as indicated in Table 2, which increases from 0·2338 to 0·6409 as S increases from zero (case 4) to one (case 6). The branches of the non-trivial parametric response for cases 5 and 6 are shown in Figure 10. From this figure, it is clear that as S is increased, these response branches are reduced in amplitude, while the main region of instability is widened.

In the superharmonic resonant case ($\Omega \approx 0.5$), the parameter S has a very interesting influence on the response. When the frequency Ω is near to 0·5, the amplitude of the homogeneous solution depends on the length ratio and the mass ratio. From equation (78), it is seen that the overall amplitude of this superharmonic response decreases as the mass ratio increases from 0 to a critical value, which is about 0·11, while this amplitude increases as the mass ratio increases beyond this critical value. Hence, it is possible to suppress the contribution of this resonance by choosing the mass ratio properly. The amplitude of the response at $\Omega = 0.50$, varied as a function of S as determined from AUTO is shown in Figure 11. From this figure, it is clear that the numerical solution agrees in a qualitative sense with this analytical prediction, although the actual minimum occurs near $S = 1.1$.
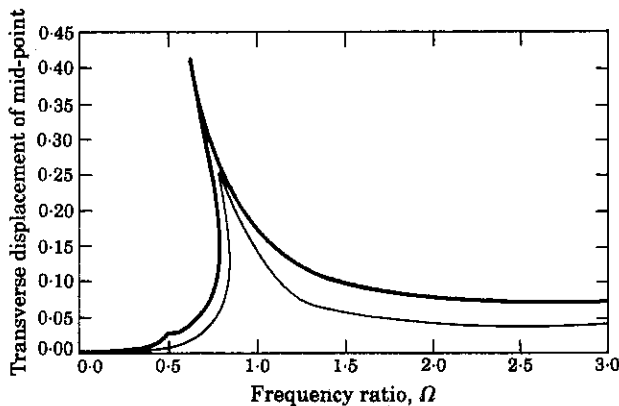

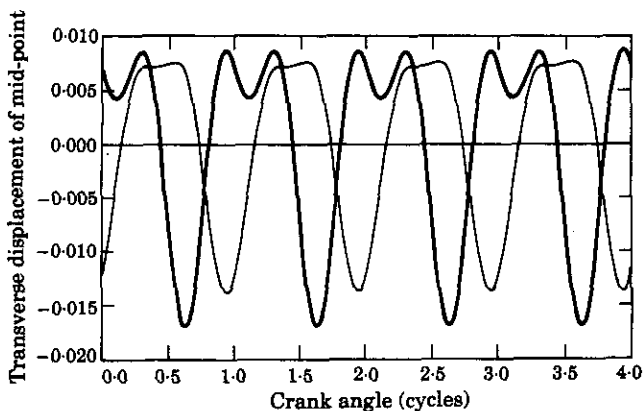Figure 12. Frequency response curves from AUTO. ——, Case 8; ——, case 10.

Figure 13. Simulation results from LSODE at $\Omega = 0.50$. ———, Case 8; ——, case 10.

4.3. EFFECT OF THE DAMPING PARAMETER μ_2

The material damping coefficient μ_2 has a favorable effect in reducing vibration amplitudes and promoting stability in all resonance regions.

The response curves for cases 8 and 10 are shown in Figure 12. From this figure, it is very clear that μ_2 has a favorable effect on the response. Moreover, all trends predicted by the analytical work are verified. A case in point is demonstrated in Figure 13, which shows that the second harmonic of the response is significantly reduced as μ_2 is increased near the $\Omega = 0.5$ superharmonic resonance.

4.4. EFFECT OF THE FRICTION PARAMETER μ_4

The effects of the slider friction are as follows: (1) near the primary resonance, increases in μ_4 reduce the amplitude and lessen the possibility of jumps occurring; (2) increases in μ_4 slightly widen the regions of parametric instability while reducing the vibration amplitude in the resonant region; (3) the amplitude of response near the superharmonic resonance is increased for large values of μ_4.

The effect of the slider friction on the connecting rod is comprised of two components. The first arises from the action of rigid body motion, while the second is caused by foreshortening. The friction force induced by the rigid body motion is linear and has an adverse effect on the response, essentially by causing an axial load on the connecting rod. The slider friction introduced by foreshortening is non-linear, and has a favorable effect
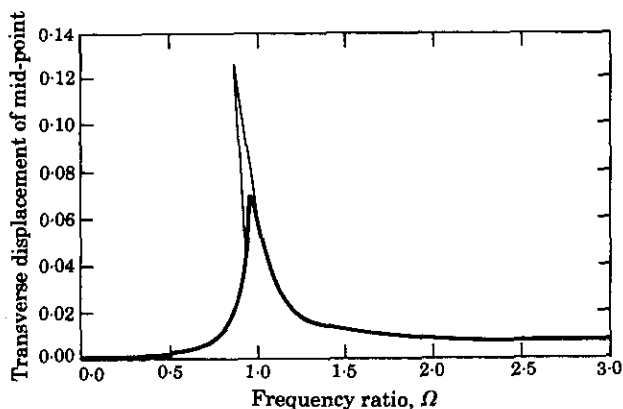

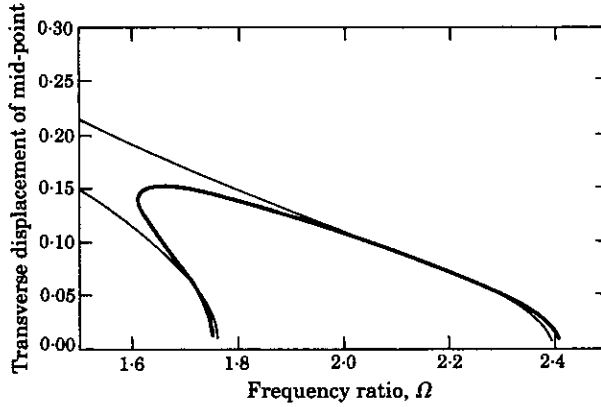Figure 14. Frequency response curves from AUTO. ———, Case 6; ——, case 11.

Figure 15. Non-trivial responses associated with the principal parametric resonance from AUTO. ———, Case 6; ———, case 11.

on the response of the system by adding damping through the shoreshortening. When the response amplitude is small, the foreshortening introduced is small, and the slider friction is mainly composed of friction induced by rigid body motion. Hence, an increase in the value of μ_4 will be accompanied with an increase of the slider friction force. This corresponds to an increase of the axial force acting on the connecting rod, and hence to an increase of the amplitude of the response. This force also promotes parametrical type instabilities. However, as the amplitude of the response increases, the friction force induced by the elastic deformation also increases. This friction force acts as a resistance to prevent the connecting rod from further elastic deformation. Hence, the friction induced by foreshortening has a favorable effect on the amplitude of the response.

The overall frequency response curves for cases 6 and 11 are shown in Figure 14. This figure shows that the friction parameter μ_4 reduces the peak amplitude of the primary resonance. In Figure 15 are shown the response branches originating from the main region of instability near $\Omega = 2$ for cases 6 and 11. From this figure, it is clear that the friction parameter μ_4 has a favorable effect on the amplitude of the principal parametric resonance, even though the width of the unstable region is slightly increased. In Figure 16 are shown the frequency response curves near $\Omega = \frac{1}{2}$ for cases 7 and 12, indicating the increase in amplitude associated with μ_4. The analytical approximations and simulation results of the response for case 12, at $\Omega = 0.50$, are shown in Figure 17. Near this resonance, as μ_4 is
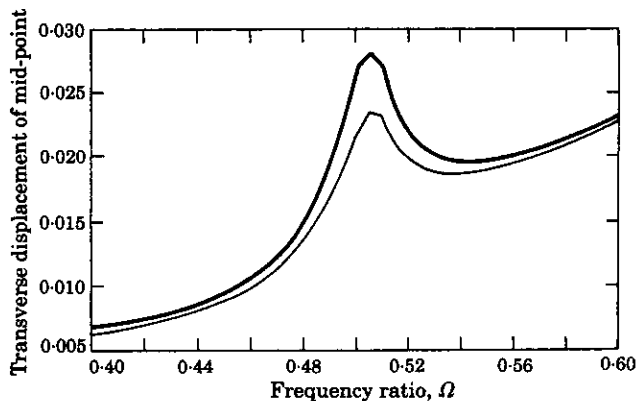

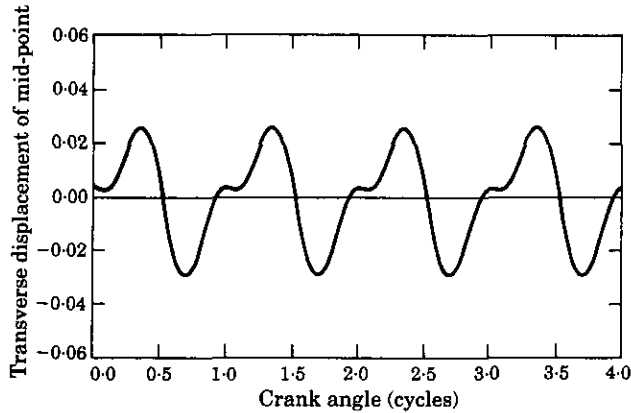Figure 16. Frequency response from LSODE. ———, Case 7; ———, case 12.

Figure 17. Analytical approximation and simulation results for case 12. ——, MMS; ——, LSODE.

increased, the amplitude of the second harmonic increases, demonstrating that the perturbation approach provides very accurate results when compared with the numerical solutions.

4.5. EFFECT OF THE FREQUENCY RATIO Ω

In order to understand the influence of Ω on the response of the system, it is convenient to separate the discussion into three categories; low frequency ratios, non-resonant frequency ratios and resonant frequencies ratios.

First, consider the low frequency ratio region. The inertial forces applied to the system, due to the accelerations a_x and a, are proportional to Ω^2. However, since the system is non-linear, this does not necessarily imply that the amplitude of the steady state response is proportional to Ω^2.

For small values of Ω and ξ, equation (21) yields a satisfactory approximation given by

$$X = \frac{2}{\pi} \frac{\xi\Omega^2}{\sqrt{(1 - \Omega^2)^2 + 4\mu_2^2\Omega^2}} \approx \frac{2}{\pi} \xi\Omega^2 \qquad (79)$$

for $\Omega \ll 1$. This implies that the amplitude of the response is proportional to $\xi\Omega^2$ in this parameter range. This point has been made by previous investigators [10]. The response for large ξ and small Ω remains to be considered.

Next, consider the non-resonant cases. When no resonance is excited, the free oscillation term will decay to zero due to the presence of the damping. Consequently, the linear approximation will be sufficient to provide a good estimate of the response.

When a resonance occurs at a given operating frequency, an additional harmonic (or harmonics) must be included in order to capture the effect of the homogeneous solution. Therefore, additional peaks appear along the profile of the linear response curve. This paper is essentially a characterization of these resonance cases.

It is interesting to consider the series expansion of the kinematic constraint given in equation (18). From this expansion, it is clear that the applied force is composed of multiple frequencies. Generally speaking, when Ω is near to $1/n$, a superhamonic resonance is expected to arise. It is difficult to analytically study these higher order ($n > 3$) superharmonic resonances, since the magnitude of the homogeneous solution is proportional to the corresponding order of the length ratio, i.e., ξ^n. Unless the length ratio is quite large, the contribution of the homogeneous solution on the steady state response will be very small. This also explains the absence of these higher order resonances in the simulation results.

5. CONCLUSIONS

The results presented in this work represent a successful extension of previous efforts, in that the effects of non-linearities on the vibration response of a flexible connecting rod have been analyzed in a systematic manner. The major drawbacks of this approach are that tedious manipulations are involved in analyzing the higher order resonances and that only limited parameter ranges can be handled (e.g., $\xi < 0.1$). With the advent of high speed computers, the finite element approach has become more favorable for specific design purposes. However, like most numerically based approaches, the finite element approach can only provide pointwise information in parameter space. A recent finite element study [30] used more than 100 simulations with a commercially available package to obtain a single response curve. While such an approach can provide reliable and accurate solutions, an analytical approach provides important information useful for the prediction of the influence of various parameters along with explanations of the non-linear phenomena associated with these systems.

As for the general improvement in analysis techniques for elastic mechanism problems, a more thorough understanding of the inertia force is required. In all previous analytical works, the dynamics of the flexible link are formulated relative to a co-ordinate system that follows the rigid body motion of the beam. This approach presumes infinitesimal strains and is sometimes referred to as the shadow beam approach. In future work, one should include large overall motion and strains by employing geometrically exact formulations. Recent results from Simo and Vu-Quoc [31, 32] may prove useful for this extension. Future work should also include considerations for multi-mode interactions and the possibilities of internal resonances [17].

It is clear that more systematic and thorough experimental studies of systems such as the one considered here are also in order. Recent efforts in this direction include the work of Beale, in which the influence of the length ratio and crank speed are being systematically investigated [16, 21]. In fact, some trends described by the present work have been verified by Beale, including the softening nature of the non-linearity and the appearance of the superharmonic resonance as ξ is increased.

In a complementary study [22], the authors have investigated a non-linear, distributed parameter model using similar methods and have obtained consistent results. The effect of rotary inertia and shear deformation are included in that study. The thesis by Hsieh [29] contains a detailed comparison of the results obtained by these two approaches.

REFERENCES

1. S. Chu and K. C. Pan 1975 *Transactions of the American Society of Mechanical Engineers, Journal of Engineering for Industry* **97**, 542–550. Dynamic responses of a high-speed slider–crank mechanism with an elastic connecting rod.
2. E. P. Golebiewski and J. P. Sadler 1976 *Transactions of the American Society of Mechanical Engineers, Journal of Engineering for Industry* **98**, 1266–1271. Analytical and experimental investigation of elastic slider–crank.

3. G. H. SUTHERLAND 1976 *Transactions of the American Society of Mechanical Engineers, Journal of Engineering for Industry* **98**, 788–794. Analytical and experimental investigation of a high-speed elastic-member linkage.
4. B. V. VISCOMI and R. S. AYRE 1971 *Transactions of the American Society of Mechanical Engineers, Journal of Engineering for Industry* **93**, 251–262. Nonlinear dynamics response of elastic slider–crank mechanism.
5. A. G. ERDMAN and G. N. SANDOR 1972 *Mechanism and Machine Theory* **7**, 19–33. Kineto-elastodynamics—a review of the state of the art trends.
6. G. G. LOWEN and W. G. JANDRASITS 1972 *Mechanism and Machine Theory* **7**, 3–17. Survey of investigation into the dynamic behavior of mechanisms containing links with distributed mass and elasticity.
7. G. G. LOWEN and C. CHASSAPIS 1986 *Mechanism and Machine Theory* **21**, 33–42. The elastic behavior of linkages: an update.
8. B. S. THOMPSON and C. K. SUNG 1986 *Mechanism and Machine Theory* **21**, 351–359. A survey of finite element techniques for mechanism design.
9. A. H. NEUBAUER, JR., R. COHEN and A. S. HALL, JR. 1966 *Transactions of the American Society of Mechanical Engineers, Journal of Engineering for Industry* **88**, 311–317. An analytical study of the dynamics of an elastic linkage.
10. P. W. JASINSKI, H. C. LEE and G. N. SANDOR 1970 *Journal of Applied Mechanics* **37**, 1069–1076. Stability and steady-state vibrations in a high-speed slider–crank mechanism.
11. P. W. JASINSKI, H. C. LEE and G. N. SANDOR 1971 *Transactions of the American Society of Mechanical Engineers, Journal of Engineering for Industry* **93**, 636–644. Vibration of elastic connecting rod of a high-speed slider–crank mechanism.
12. M. BADLANI and W. KLEINLENZ 1979 *Transactions of the American Society of Mechanical Engineers, Journal of Mechanical Design* **101**, 149–153. Dynamic stability of elastic mechanisms.
13. I. G. TADJBAKHSH 1982 *Transactions of the American Society of Mechanical Engineers, Journal of Mechanical Design* **104**, 698–703. Stability of motion of elastic planar linkage with application of slider–crank mechanism.
14. Z. G. ZHU and Y. CHEN 1983 *Transactions of the American Society of Mechanical Engineers, Journal of Mechanisms, Transmission, and Automation in Design* **105**, 637–640. The stability of the motion of a connecting rod.
15. M. BADLANI and A. MIDHA 1983 *Transactions of the American Society of Mechanical Engineers, Journal of Mechanisms, Transmission, and Automation in Design* **105**, 452–459. Effect of internal material damping on the dynamics of a slider–crank mechanism.
16. D. G. BEALE and S.-W. LEE 1991 *Proceeding of 13th ASME Conference on Mechanical Vibration and Noise DE-Vol.* 37, *Miami, Florida*, 161–166. Investigation of parametric resonance instability in a flexible rod slider–crank mechanism.
17. K. FARHANG and A. MIDHA 1991 *Proceeding of 13th ASME Conference on Mechanical Vibration and Noise DE-Vol.* 37, *Miami, Florida*, 167–176. Investigation of parametric vibration stability in slider–crank mechanism with elastic coupler.
18. K. FARHANG and A. MIDHA 1989 *Proceedings of the First National Applied Mechanisms and Robotics Conference I, Cincinnati, Ohio*, 3B-7-1–3B-7-7. A model for studying parametric stability in slider–crank mechanisms with flexible coupler.
19. A. I. MAHYUDDIN, A. MIDHA and A. K. BAJAJ 1990 *Cams, Gears, Robot and Mechanisms Design.* New York: ASME; also *21st Biennial ASME Mechanisms Conference, Chicago, Illinois, DE-Vol.* 26, 1–9. On methods for evaluation of parametric stability and response of flexible cam–follower systems.
20. A. I. MAHYUDDIN and A. MIDHA 1990 *Cams, Gears, Robot and Mechanisms Design.* New York: ASME; also *21st Biennial ASME Mechanisms Conference, Chicago, Illinois, DE-Vol.* 26, 11–21. Influence of varying cam profile and follower motion event types on parametric stability.
21. D. G. BEALE and S.-W. LEE 1992 *Nonlinear Dynamics* (in press). Steady state response of a slider crank with flexible rod.
22. S. HSIEH and S. W. SHAW 1991 Dynamic stability and nonlinear resonance of a flexible connecting rod: continuous parameter model (submitted for publication).
23. T. R. KANE, P. W. LIKINS and D. A. LEVINSON 1983 *Spacecraft Dynamics.* New York: McGraw-Hill.
24. T. R. KANE and D. A. LEVINSON 1981 *The Journal of Astronautical Science* **29**, 213–244.
25. V. K. KUMAR and P. M. BAINUM 1980 *Journal of Guidance and Control* **3**, 90–91. Dynamics of a flexible body in orbit.

26. A. H. NAYFEH and D. T. MOOK 1979 *Nonlinear Oscillations*. New York: Wiley Interscience.
27. A. C. HINDMARSH 1983 *Scientific Computing* (R. S. Stepleman, editor), 55–64. Amsterdam, North-Holland. Odepack, a systematized collection of ode solvers.
28. E. DOEDEL 1981 *Congressus Numerantium* **30.** Auto: a program for the automatic bifurcation analysis of autonomous systems.
29. S. HSIEH 1991 *Ph.D. Thesis, Michigan State University*. Nonlinear vibrations of a flexible connecting rod.
30. D. L. CRONIN and H. LIU 1989 *The First National Applied Mechanisms and Robotics Conference, Cincinnati, Ohio*. Finite element analysis of the steady-state behavior of flexible mechanisms.
31. J. C. SIMO and L. VU-QUOC 1986 *Transactions of the American Society of Mechanical Engineers, Journal of Applied Mechanics* **53**, 849–854. On the dynamic of flexible beam under large overall motions—the plane case: part I.
32. J. C. SIMO and L. VU-QUOC 1986 *Transactions of the American Society of Mechanical Engineers, Journal of Applied Mechanics* **53**, 855–863. On the dynamic of flexible beam under large overall motions—the plane case: part II.